ADVANCED OPTICAL MATERIALS
www.advopticalmat.de

Silicon Microspheres for Super-Planckian Light Sources in the Mid Infrared

Roberto Fenollosa, Fernando Ramiro-Manzano, Moises Garín, and Francisco Meseguer*

Silicon microspheres with a diameter in the range of 2–3 micrometers constitute photonic nanocavities that emit light through their Mie resonances when heated at high temperatures. At 500–600 °C these microresonators show a particular mid-infrared (MIR) emission dominated by the lowest order modes. Such resonances feature a large free spectral range, about 600 cm^{-1}, and a high proximity to the critical coupling condition. In fact, resonances with high-quality factor, around 160 are found. It corresponds to the limit of detection of their measuring setup, being 600 the theoretical value. Most importantly, several modes emit light above the calculated black body limit because they feature an optical absorption cross-section larger than their geometric one. All these characteristics set silicon microspheres as very promising zero-dimensional materials for developing micrometric and sub-wavelength light sources in the MIR.

1. Introduction

Thermal emission is a fundamental physical phenomenon occurring in every day's life. It consists of the radiation of light by an object by virtue of its temperature. Usually, such radiation is emitted to all directions of space and it extends to a broadband spectral range peaked, for instance, around 10 micrometers of wavelength, λ, for a body at 25 °C. The rise of temperature, T, increases substantially the total radiation intensity and shifts the emission peak towards shorter wavelengths, according to the Stefan–Boltzmann and Wien laws[1,2] respectively. The thermal emissive power at a certain λ of a bulk body equals that of a black body (Planck law) corrected by the emissivity factor, e, according to the following equation:

$$I = \frac{2\pi hc^2}{\lambda^5 \exp\left(\frac{hc}{\lambda kT} - 1\right)} e \tag{1}$$

In addition, there is reciprocity between the emission and absorption of light by virtue of Krichoff law,[3,4] i.e., at a certain wavelength, a good emitter is a good absorber.

From a fundamental point of view and for some technological applications it is interesting to tailor such a broad emission spectrum into a more defined one with desired characteristics.[5] A key feature is the spectral bandwidth, i.e., the temporal coherence. A certain degree of control in this regard can be very useful, for instance, for improving the efficiency of devices in the field of solar thermophotovoltaics,[6] for radiative cooling,[7] and for nondispersive gas sensing.[8,9] In principle, narrow-band thermal emission could be achieved by heating a gas of molecules because they would emit light mainly at those frequencies corresponding to their bond vibration. Consequently, the wavelength of emission could be tuned to a certain point by modifying the gas composition. However, this is technologically unpractical, and therefore other strategies have been applied such as the use of different solid-state equivalents like rare-earth oxides[10] and low dimensional (1D and 2D) structures with quantum confinement.[11,12] These approaches have provided thermal emissions with narrow features mainly in the visible and near-infrared (NIR) ranges. Additionally, calculations have shown that a thin layer of SiC could yield narrow emission in the reststhralen band, around 10 micrometers of wavelength.[13]

A more fruitful approach is to design the material geometry with the purpose of converting the broad spectral emissivity into a scenario of narrow and discrete frequency bands. In this way and with the help of nanotechnology, several developments have been proposed: one of the solutions consists of the introduction of multiple quantum wells in a photonic crystal. As a consequence, thermal emission consisting of a single peak with a quality factor (Q) of 100 was achieved around 1000 cm^{-1}.[14] Other approaches have focused on metamaterials for engineering compact gas sensors whose light source provides a narrow mid-infrared (MIR) emission.[9,15,16] Finally, the utilization of the optical resonances of micrometer size bodies with an appropriate geometry has proven to be very useful for achieving narrow peaked thermal emissions. This is the case of an optical antenna[17] based on

R. Fenollosa, F. Ramiro-Manzano, F. Meseguer
Instituto Universitario de Tecnología Química, CSIC-UPV, Universitat Politècnica de València
Av. dels Tarongers
València 46022, Spain
E-mail: rfenollo@ter.upv.es
M. Garín
GR-MECAMAT, Universitat de Vic – Universitat Central de Catalunya (UVIC-UCC)
Campus Torre dels Frares
c/ de la Laura 13, Vic 08500, Spain

The ORCID identification number(s) for the author(s) of this article can be found under https://doi.org/10.1002/adom.202300135

DOI: 10.1002/adom.202300135

cylindrical SiC whiskers, that yielded a peaked emission with a Q of 27.

In this context, we reported some time ago about the thermal emission of silicon microspheres.[18] They yielded emission spectra with well-defined peaks that originated from Mie resonances, and a Q of 400 was measured in the NIR range (700 to 2000 nm). This achievement was remarkable and of technological interest because the NIR range includes some biological and telecommunications windows. However, theoretical calculations showed that such structured spectral emission continued to the MIR (2 to 20 μm) with more exciting features and promising opportunities. To start with, silicon microspheres were expected to show in this range a sub-wavelength character producing striking phenomena such as emission above the Planck limit. On another hand, the MIR corresponds to that wavelength range where the chemical print of most species appears, and it includes atmosphere transparency windows (3-5 and 8–14 μm). Therefore, improvements in this range could have important consequences in areas such as chemical detection and radiative cooling. Moreover, the development of photonic chips in the MIR is still at the starting stages, and MIR light sources at the micrometer size level, with the appropriate performance are scarce and very expensive. Consequently, new strategies in this regard could be of special interest. Finally, from an experimental point of view, the measurement of thermal radiation of a micrometer size body is much more challenging than the measurements in the VIS or NIR ranges and, as we will see below, has required the development of appropriate interferometry tools that could be helpful for other scientists working in similar areas. Hereafter, we report on the thermal emission of silicon microspheres in the MIR.

2. Results and Discussion

2.1. Microspheres Morphology and Bespoke FTIR Measurement System

Silicon microspheres were synthesized by chemical vapor deposition using di-silane gas as a precursor, and appropriately crystallized afterward (see Methods).[19] Therefore, they have a polycrystalline nature.[20] **Figure 1** shows an SEM image of several microspheres. Because of their high sphericity, smooth surface, and high refractive index they behave as photonic nano-cavities, able to trap light efficiently in a very small volume. The image illustrates the small contact point between the microspheres and the substrate. This is a key feature for achieving high temperatures with relatively low laser irradiation intensities because it helps reducing the heat release to the substrate by conduction.[18]

Thermal emission measurements of micrometer-size bodies in the MIR are very challenging because of the small emitted intensities and the requirement of isolating those target signals from the MIR emission of the surrounding environment. For that purpose, we developed a bespoke Fourier transform infrared spectrometer (FTIR) (**Figure 2**) with a lock-in detection system. In particular, the heat source, that is based on a blue laser, is modulated at a certain frequency. This modulation affects only to those signals originated from the sphere because first, the source is focused on it and second its fast dynamics allows to respond to that frequency.[18] As a consequence, the isolated signal of the modulated amplitude of the target sphere is synchronously acquired.

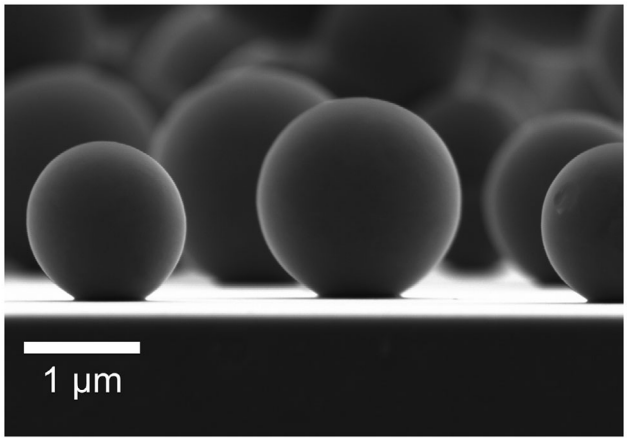

Figure 1. SEM image showing a side view of as-synthesized polycrystalline silicon microspheres.

In addition, a feedback control is implemented for stablishing a precise wavelength accuracy (see Methods).

2.2. Mie Theory Based fit of Thermal Emission Spectra

The measured thermal emission spectra in the MIR of two polycrystalline silicon microspheres are shown in **Figure 3**a,b (black curves). They have different diameters (**Table 1**) that were determined by fitting their optical scattering at 90 degrees in the visible and near-infrared ranges.[19] We call them as M1 and M2 from now on.

The red curves correspond to the fits of the experimental data to Equation (1), considering the emissivity equals the absorption efficiency (q_{abs}) of the microsphere,[21] provided by Mie theory, where q_{abs} is the optical absorption cross-section divided by the projected geometric area ($A = \pi r^2$), r being the sphere radius. The main fitting parameter is the temperature (Table 1), which not only appears in the black body term but it also influences the optical constants of the silicon particle and thus the emissivity itself. Additionally, two parameters, not shown in the table, were used to account for the normalization and offset of the experimental data. The rise of temperature produces mainly an increment in both the real, n, and the imaginary, k, parts of the refractive index and in turn of q_{abs}. While the increase in n shifts the resonances towards longer wavelengths[22] (thermo optic effect), the increment of k shifts in the same way the position of the electronic band gap.[18] In the calculations, we have assumed that the main contribution to the increase of k comes from the increment of free carriers[23–25] (FC from now on). The contribution of lattice vibration that should appear for silicon in the range from 6 to 25 μm has been disregarded because at the working temperatures of the experiments it is considered to be shadowed by the strong presence of the FC.[26] The Supporting Information contains additional details about the assumptions considered in the calculations. The results show a fairly good agreement between theory and experiments, which allowed us to associate the peaks with Mie resonances. In order to identify which resonance corresponds to each peak calculations including a single multipole of the Mie series[21] were performed. The resonances have been indicated in the figure with the usual nomenclature for Transverse

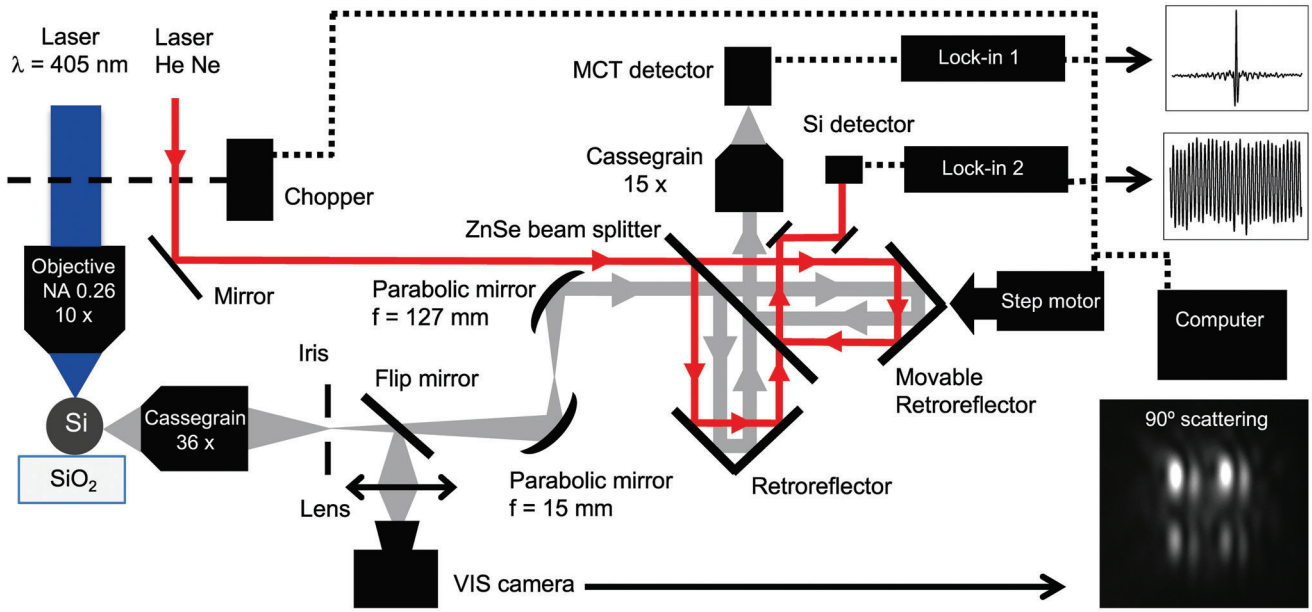

Figure 2. Schematic of the experimental setup for thermal emission measurements on individual silicon microspheres. A blue laser focused on the microsphere works as a heat source by taking advantage of the absorption of light by silicon at that wavelength. Visible light (not shown) scattered at 90° by the microsphere and a visible camera helps positioning a 36x Cassegrain objective (see scattering pattern in the inset). Mid-infrared light emitted by the microsphere is guided by two parabolic mirrors to an interferometer consisting of two retroreflectors, one of them movable by a step motor, and a ZnSe beam splitter. At the same time, light coming from an HeNe laser is introduced in the interferometer for calibration purposes of the retroreflector displacement. Light emitted by the microsphere is focused on a MCT detector by a 15× Cassegrain objective at the output of the interferometer while the HeNe laser light is guided to a Si detector. Both lasers are modulated by a chopper at 630 Hz, and the corresponding signals acquired by using two lock-in amplifiers.

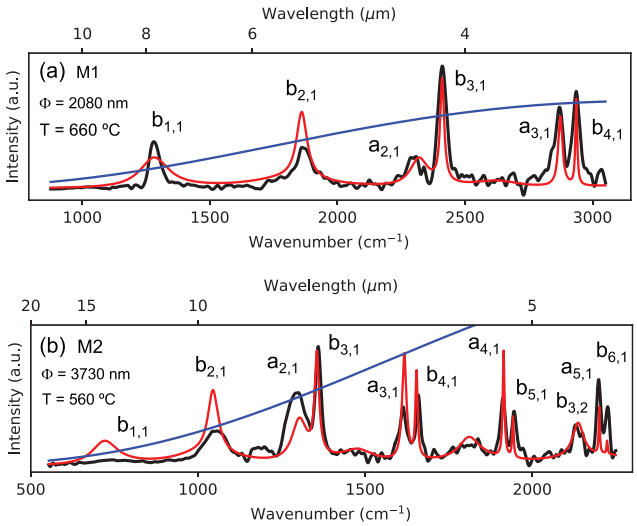

Figure 3. a) Measured thermal emission spectrum (black line) of a silicon microsphere with 2080 nm in diameter. The red curve corresponds to the fit of the experimental data to Equation (1) with a fitted temperature of 660 °C (M1 in Table 1). The blue line is the calculated emission of a black body that has an area equal to the geometric projected area of the microsphere. The modes associated to each peak are indicated. b) Same as (a) but for a 3730 nm in diameter microsphere with a fitted temperature of 560 °C (M2 in Table 1).

Table 1. Diameter values (Φ) and fitted temperatures of studied silicon microspheres.

Microsphere Name	Φ (nm)	*T* (°C)
M1	2080 ± 5	660 ± 13
M2	3730 ± 5	560 ± 10

Magnetic (a's) and Transverse Electric (b's) modes.[27] In some cases, for instance for $a_{1,1}$ and $b_{1,2}$ resonances of M1, the associated peak is too weak to produce an appreciable feature in the spectrum and they have not been specified. Nevertheless, they should contribute to the total emission. A more detailed explanation of the resonance identification procedure as well as measurements performed on other microspheres can be found in the Supporting Information.

The measured spectral range contains the lowest number modes in the studied microspheres. Although such types of resonances had already been measured by optical transmission,[28] this is the first time they are measured via thermal emission. Notable features of the resonances are their high proximity to the *Q* matching condition and the large free spectral range (FSR), i.e., the distance between consecutive modes. The *Q* matching condition or critical coupling is very important for obtaining a strong emission and it is achieved in thermal emission to free space when $Q_{rad} = Q_{abs,}$ where Q_{rad} and Q_{abs} correspond to the quality factor associated to intrinsic radiative curvature losses and to those losses produced by the material absorption respectively.

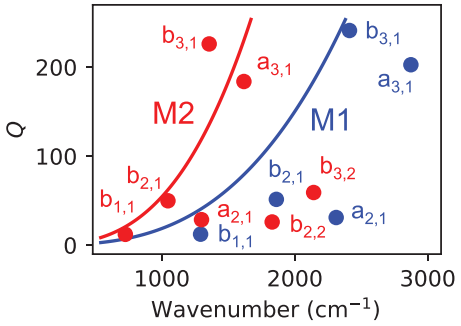

Figure 4. Calculated quality factor associated with absorption, Q_{abs}, (blue and red lines), and with intrinsic radiative curvature losses, Q_{rad} (blue and red dots) for several modes of M1 and M2 respectively. They are close to the critical coupling condition ($Q_{rad} = Q_{abs}$).

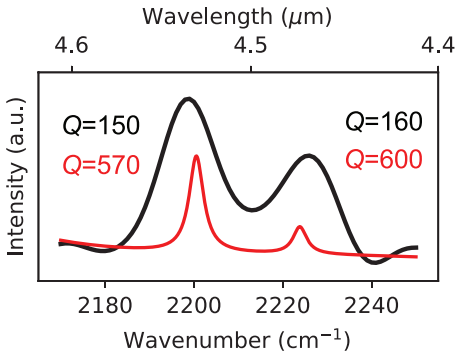

Figure 5. The zoomed spectral zone corresponding to modes $a_{5,1}$ and $b_{6,1}$ of M2. The *Q*-values obtained by fitting the experimental (black line) and theoretical (red line) spectra to a curve consisting of the summation of two lorentizans are indicated beside each peak.

Figure 4 shows Q_{abs} in blue and red lines for M1 and M2 respectively. They were calculated from the following equation:[29–31]

$$Q_{abs} = \frac{2\pi n}{\lambda \alpha} \tag{2}$$

where α is the absorption coefficient. As expected, Q_{abs} shows lower values for M1 than for M2 because of its higher temperature that gives rise to a larger absorption coefficient. On the other hand, Figure 4 indicates with dots Q_{rad} values for those modes which are near the critical coupling condition. They were obtained by fitting the theoretical scattering spectra, assuming there is no absorption, of each mode to a Lorentzian curve in order to extract the center position and the width of the corresponding peak. Finally, the measurable total *Q* of a resonance is:[32]

$$\frac{1}{Q} = \frac{1}{Q_{rad}} + \frac{1}{Q_{abs}} \tag{3}$$

where we disregard any losses related with residual surface inhomogeneities and contaminants.

The FSR reached a value around 600 cm^{-1} for the first two modes of M1, and their widths are about 100 cm^{-1}, yielding *Q's* in the order of magnitude of 10. Nevertheless, resonances with much higher *Q* could be found at larger wavenumbers. **Figure 5** shows the zoomed area of Figure 3b corresponding to modes $a_{5,1}$ and $b_{6,1}$ of M2. The fit of the experimental spectrum (black line) to the superposition of two Lorentzian curves yielded *Q* values of 150 and 160, respectively. They are, however, limited by the resolution of our setup, which is in this case about 11 cm^{-1}. In fact, their theoretical counterparts have *Q*'s of 570 and 600, respectively (see Supporting Information).

Although such high *Q* resonances are far from the critical coupling condition, a more optimum coupling could be achieved, for instance, by placing the emitting microsphere at a certain distance from a waveguide,[33] although at the expense of reducing the total *Q*, or by tuning the temperature and the microsphere diameter. This would be an important step toward the realization of MIR sources in integrated devices. In this sense, monolithic on-chip schemes such as those based on semi-isolated silicon microspheres should be remarked.[34] In addition, it has been shown that thermal emission could be substantially enhanced in the near field.[35,36] This is, however, out of the scope of this work and it constitutes a current research goal.

2.3. Super-Planckian Emission

The most striking feature for both microspheres, M1 and M2 is that there are several modes radiating above the Planck limit (also called as super-Planckian emission) which has been indicated by the blue curves in Figure 3a,b. This is a theoretical result based on the fact that the optical absorption area is larger than its projected geometric area,[21,37] i.e., $q_{abs} > 1$. On the other hand, it should be stressed that this result does not violate the Planck law which assumes that the radii of curvature of the surfaces under consideration are large compared with the wavelengths of the rays considered. In any case, the emission above the Planck limit occurs in all dimensions of space, thus setting silicon microspheres as a promising platform for undertaking further experiments in this field. To our knowledge, there have been few reports in this regard, all of them concerning 2D[38–40] or 1D[17,41] systems.

Because super-Planckian emission occurs whenever $q_{abs} > 1$ and the temperature is the main factor determining the absorption (predominantly via free carriers), a given resonance could radiate above or below the Planck limit depending on the microsphere temperature. Nevertheless, other methods such as the introduction of dopants could be utilized as well for tuning the absorption. Another criterion for predicting whether a resonating mode will reach super-Planckian emission consists of considering the scattering efficiency (q_{sca}) of the microsphere assuming no absorption losses, i.e., by setting the imaginary part of the refractive index, *k*, to zero. Then, calculations have shown that $q_{abs} = q_{sca}(k = 0)/4$ at *Q*-matching condition.[29] Therefore, the Planck limit will be surpassed for those resonant peaks where $q_{sca} > 4$. **Figure 6** shows the calculated scattering efficiency for a silicon microsphere with diameter equal to that of M1 (Φ = 2080 nm) at zero absorption in an extended spectral range. The dashed red line specifies the limit above which a resonance is, in principle, a candidate for achieving super-Planckian emission. It can be achieved by many resonances which have been indicated in the figure. However, the maximum q_{abs} is expected for the lowest number and order ones, specially for $b_{1,1}$ which has a relatively low *Q*. Other higher number modes which are placed at shorter wavelengths could, in principle, yield super-Planckian emission as well. However, they have a much higher *Q*, and therefore a

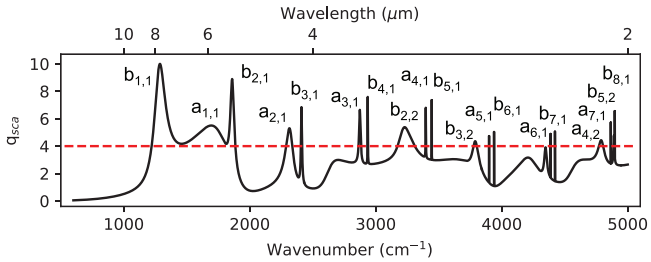

Figure 6. Calculated scattering efficiency, q_{sca}, of a silicon microsphere with a diameter of 2080 nm (equal to that of M1) at zero absorption. The dashed red line indicates the limit above which a resonance can yield emission above the Planck limit as long as it is at *Q*-matching condition. These resonances have been indicated beside their corresponding peak.

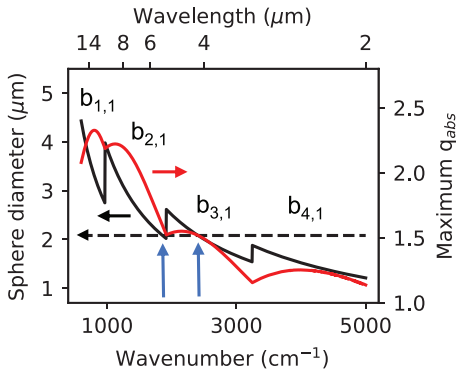

Figure 7. Calculated sphere diameter (black line) that maximizes the absorption efficiency, q_{abs}, (red line) at the temperature of the M1 experiment (660 °C). It is achieved in several spectral sections through different indicated resonances. The dashed line specifies the sphere diameter of M1 (2080 nm). The intersections with the continuous black line, indicated by the blue arrows, correspond with resonances $b_{2,1}$ and $b_{3,1}$ of Figure 3a and they indicate that maximized emission has been achieved at those spectral positions.

much lower-temperatures would be required in order to increase Q_{abs} and be able to achieve the *Q*-matching condition. This could hinder, however, the detection because of the low emitted power.

The spectral position of the Mie modes is determined by the microsphere diameter. This is the reason why the resonances of M1 (with a diameter smaller than that of M2), are blue-shifted with respect to those of M2. Therefore, at a given temperature and wavelength there is expected to be a microsphere diameter that maximizes q_{abs} and thus the emission intensity. **Figure 7** shows these calculations in an extended wavelength range (black and red curves respectively) for the temperature of M1 experiment (660 °C). Both curves have a discontinuous behavior thus dividing the calculated values into several sections because the maximum q_{abs} is achieved through different indicated resonances. The dashed black line specifies the sphere diameter of M1 (2080 nm). The figure shows clearly that this is not an appropriate diameter for maximizing the emission neither with a $b_{1,1}$ nor with a $b_{4,1}$ resonance although in both cases the emission occurs above the Planck limit (see Figure 3a). The emission is maximized, on the other hand, at $b_{2,1}$ and $b_{3,1}$ resonances at those wavenumbers coinciding with the intersections (indicated by the blue arrows) between the dashed and the continuous black lines with an intensity of about 1.5 times that of the black body.

Based on the equivalence between q_{abs} and the emissivity, Figure 7 shows that the maximum achievable surpass of the Planck limit at 660 °C is 2.3 approximately and it can be reached around 800 cm^{-1} with a sphere diameter of 3300 nm using $b_{1,1}$ resonance. Other systems, like those based on plasmon resonances for instance, could in principle surpass the Planck limit to a higher extent. Calculations from the literature have shown that q_{abs} can reach values near 4 and even 14 for gold nanospheres and nanorods respectively.[42] However, the wavelengths where this could be attainable correspond to the VIS and the NIR ranges. Therefore, temperatures much higher than those used here, probably near the melting point of the nanoparticles, would be required, thus hampering the experiments. On another hand, in general, plasmon resonances of metal nanostructures are usually much broader than the Mie modes of silicon microspheres, thus emission peaks would probably be much less defined.

3. Conclusion

The thermal emission spectra of silicon microspheres in the mid-infrared show well-defined peaks that were associated with Mie resonances. They have notable features, namely a large FSR, a high proximity to the *Q*-matching condition, the appearance of high *Q*-modes, and the possibility of radiating above the Planck limit in the three dimensions of space. That makes them a very promising platform for undertaking fundamental studies of heat transfer by thermal radiation and for developing light sources in the mid-infrared.

4. Experimental Section

Synthesis of Silicon Microspheres: Silicon microspheres were synthesized in a closed reactor with controlled conditions of temperature and pressure. Di-silane, the precursor gas, was introduced in the reactor at a pressure of 15 kPa and heated at 420 °C for 30 min. The as-synthesized microspheres were composed by amorphous silicon and they were submitted to a slow crystallization treatment[19,27] at 800 °C. Single microspheres from the supporting substrate (based on silicon) utilized for the synthesis and crystallization processes were picked up by micromanipulation means and positioned on a glass substrate for the thermal emission measurements. We ensured that they were well separated from each other (typical separation distance was several tens of micrometers) in order to avoid any interference effect between them.

The diameter measurements were realized after the thermal emission experiments by optical scattering measurements in the VIS and NIR ranges.[19] In principle, we have discarded the formation of any SiO_2 coating layer on the silicon microspheres surface by the laser heating because the emission temperatures are below those where appreciable oxidation rates occur.[43] Nevertheless, in case such a layer grew it would be equivalent to a reduction of the sphere diameter because of the low refractive index of SiO_2 and it would be in agreement with the diameter values obtained by optical scattering. Therefore, deviations of the fitted temperatures from those of the "true" values associated with this phenomenon are not expected.

FTIR Measurements: Similarly to previous experiments,[18] the microspheres were placed on a glass substrate in air and they were heated by means of a blue laser (λ = 405 nm, power 5 ≈ mW). However, in order to remove unrelated thermal contributions the measurements were realized by chopping the excitation light at a certain frequency, in this case, 630 Hz, and the signal was recorded with the help of a liquid nitrogen refrigerated MCT detector connected to a lock-in amplifier. The small size of the microspheres featuring microsecond response in the heating and cooling processes,[18] has allowed this detection scheme. The thermal

light emitted by a microsphere is captured by a high magnification (36x) Cassegrain objective and guided to an interferometer consisting of two retro-reflectors, one of them movable by a step motor attached to a linear stage micrometer platform, and a 3 mm thick ZeSe window that works as a beam splitter (Figure 2). We used additionally the scattering at 90° of white light and a visible camera for focusing properly the Cassegrain objective on the microsphere. An inset in the figure illustrates such dark-field imaging. The two upper lobes correspond to the scattering at the sphere borders while the two lower lobes are their reflected image through the substrate. At difference with measurements performed in the visible and near-infrared ranges, here we did not limit the image field to an area that is tangential to the microsphere border,[19] rather we kept the iris totally opened during the measurements. Therefore, we expect to record the signal originated from resonances in all the planes, included those crossing the substrate. Finally, it was very important to calibrate the displacement of the movable retro-reflector by measuring the interference pattern of a source with a known wavelength such as a HeNe laser. For that purpose, the obtained interferogram from the thermal emission was compared with the interference pattern of the HeNe laser and appropriately corrected before realizing the Fourier transform for obtaining the corresponding spectrum (see Supporting Information).[44] All the system was driven by homemade software.

Interferograms were acquired by scanning the movable retroreflector around the zero retardation point. While the blue and red lasers were being chopped at a frequency of 630 Hz, the motor moved at a 3 ms per step. The intensity originated from the sample and from the calibration laser were averaged at 10 and 1 s, thus providing measurement points every 2.6 and 0.26 μm, respectively. The maximum retardation of the interferograms for M1 and M2 was ±600 and ±900 μm. The measurements took 76.8 and 115.2 min and provided a resolution of 17 and 11 cm^{-1}, respectively. Such long integration times are necessary for removing the considerable noise from the small intensity signal radiated. However, problems related with the stability of the alignment of all the system, specially those corresponding to the blue laser and the sample prevents from achieving a higher resolution. We are currently working to improve this point.

Fitting Process: Weighted Orthogonal Distance Regression[45] was used for fitting all of the emission spectra because it allows handling errors in both *x*- and *y*-axis. We considered an error of 20 cm^{-1} in the wavenumber of the experimental data (*x*-axis) to account for miscalibration effects of the spectrometer and for inaccuracies that may exist in the determination of the refractive index of silicon at high temperatures. The uncertainty in the intensity (*y*-axis) was set at the square root of the number of counts. The fitted parameter uncertainties correspond to the square root of the diagonal covariant matrix elements resulting from the fitting process.

Supporting Information

Supporting Information is available from the Wiley Online Library or from the author.

Acknowledgements

This work was supported by several projects of the Spanish Ministry of Science, Innovation, and Universities: PLEC2021-007576, and Severo Ochoa Centre of Excellence Program (CEX2021-001230-S).

Conflict of Interest

The authors declare no conflict of interest.

Data Availability Statement

The data that support the findings of this study are available from the corresponding author upon reasonable request.

Keywords

microspheres, mid-infrared, Mie resonances, nano-cavities, silicon, super-Planckian

Received: January 17, 2023
Revised: March 24, 2023
Published online:

[1] M. F. Modest, *Radiative Heat Transfer*, Academic Press, New York **2013**.
[2] M. Planck, *The Theory of Heat Radiation*, P. Blakiston's Son & Co., Philadelphia **1914**.
[3] D. B. Brace, *The Laws of Radiation and Absorption: Memoirs by Prévost, Stewart, Kirchhoff, and Kirchoff and Bunsen*, American Book Company, New York **1901**.
[4] D. A. B. Miller, L. Zhu, S. Fan, *Proc. Natl. Acad. Sci.* **2017**, *114*, 4336.
[5] D. G. Baranov, Y. Xiao, I. A. Nechepurenko, A. Krasnok, A.l Alù, M. A. Kats, *Nat. Mater.* **2019**, *18*, 920.
[6] Z. Zhou, E. Sakr, Y. Sun, P. Bermel, *Nanophotonics* **2016**, *5*,1.
[7] A. P. Raman, M. A. Anoma, L. Zhu, E. Rephaeli, S. Fan, *Nature* **2014**, *515*, 540.
[8] J. Hildenbrand, J. Korvink, J. Wöllenstein, C. Peter, A. Kürzinger, F. Naumann, M. Ebert, F. Lamprecht, *IEEE Sens. J.* **2010**, *10*, 353.
[9] A. Lochbaum, A. Dorodnyy, U. Koch, S. M. Koepfli, S. Volk, Y. Fedoryshyn, V. Wood, J. Leuthold, *Nano Lett.* **2020**, *20*, 4169.
[10] G. E. Guazzoni, *Appl. Spectrosc.* **1972**, *26*, 60.
[11] D. Mann, Y. K. Kato, A. Kinkhabwala, E. Pop, J. Cao, X. Wang, L. Zhang, Q. Wang, J. Guo, H. Dai, *Nat. Nano* **2007**, *2*, 33.
[12] L. Dobusch, S. Schuler, V. Prebeinos, T. Mueller, *Adv. Mater.* **2017**, *29*, 1701304.
[13] A. Narayanaswamy, J. Mayo, C. Canetta, *Appl. Phys. Lett.* **2014**,*104*, 183107.
[14] T. Inoue, M. D. Zoysa, T. Assano, S. Noda, *Opt. Express* **2016**, *24*, 15101.
[15] X. Liu, T. Talmage, T. Starr, A. F. Starr, N. M. Jokerst, W. J. Padilla, *Phys. Rev. Lett.* **2011**, *107*, 045901.
[16] A. Sakurai, K. Yada, T. Simomura, S. Ju, M. Kashiwagi, H. Okada, T. Nagao, K. Tsuda, J. Shiomi, *ACS Cent. Sci.* **2019**, *5*, 319.
[17] J. A. Schuller, T. Taubner, M. L. Brongersma, *Nat. Photonics* **2009**, *3*, 658.
[18] R. Fenollosa, F. Ramiro-Manzano, M. Garín, R. Alcubilla, *ACS Photonics* **2019**, *6*, 3174.
[19] R. Fenollosa, M. Garín, F. Meseguer, *Phys. Rev. B* **2016**, *93*, 235307.
[20] F. Meseguer, R. Fenollosa, I. Rodriguez, E. Xifré-Pérez, F. Ramiro-Manzano, M. Garín, M. Tymczenko, *J. Appl. Phys.* **2011**, *109*, 102424.
[21] C. F. Bohren, D. R. Huffman, *Absorption and Scattering of Light by Small Particles*, John Wiley & Sons, New York **1998**.
[22] J. Sik, J. Hora, *J. Appl. Phys.* **1998**, *84*, 6291.
[23] P. J. Timans, *J. Appl. Phys.* **1993**, *74*, 6353.
[24] J. C. Sturm, C. M. Reaves, *IEEE Trans. Electron. Dev.* **1992**, *39*, 81.
[25] C. D. Thurmond, *J. Electrochem. Soc.* **1975**, *122*, 1133.
[26] T. Sato, *Jpn J Appl Phys* **1967**, *6*, 339.
[27] R. Fenollosa, F. Meseguer, M. Tymczenko, *Adv. Mater.* **2008**, *20*, 95.
[28] E. Xifré-Pérez, R. Fenollosa, F. Meseguer, *Opt. Express* **2011**, *19*, 3455.
[29] M. Garín, R. Fenollosa, P. Ortega, F. Meseguer, *J. Appl. Phys.* **2016**, *119*, 033101.
[30] R. Fenollosa, M. Garín, *Mater. Sci. Semicond. Process.* **2022**, *150*, 106972.
[31] B. E. A. Saleh, M. C. Teich, *Fundamentals of Photonics*, John Wiley & Sons, New York **1991**.

[32] M. L. Gorodetsky, A. A. Savchenkov, V. S. Ilchenko, *Opt. Lett.* **1996**, *21*, 453.
[33] K. Vahala, Optical Microcavities, World Scientific, Singapore **2004**.
[34] M. Garín, M. Solà, A. Julian, P. Ortega, *Nanoscale* **2018**, *10*, 14406.
[35] K. Joulain, J. P. Mulet, F. Marquier, R. Carminati, J. J. Greffet, *Surf. Sci. Rep.* **2005**, *57*, 59.
[36] K. Kim, B. Song, V. Fernández-Hurtado, W. Lee, W. Jeong, L. Cui, D. Thompson, J. Feist, M. T. Homer Reid, F. García-Vidal, J. C. Cuevas, E. Meyhofer, P. Reddy, *Nature* **2015**, *528*, 387.
[37] Y. Xiao, M. Sheldon, M. A. Kats, *Nat. Photonics* **2022**, *16*, 397.
[38] L. Hu, A. Narayanaswamy, X. Chen, G. Chen, *Appl. Phys. Lett.* **2008**, *92*, 133106.
[39] D. Thompson, L. Zhu, R. Mittapally, S. Sadat, Z. Xing, P. McArdle, M. M. Qazilbash, P. Reddy, E. Meyhofer, *Nature* **2018**, *561*, 216.
[40] J. J. García-Esteban, J. Bravo-Abad, J. C. Cuevas, *ACS Photonics* **2022**, *9*, 3679.
[41] C. Wuttke, A. Rauschenbeutel, *Phys. Rev. Lett.* **2013**, *111*, 024301.
[42] P. K. Jain, K. S. Lee, I. H. E-Sayed, M. A. El-Sayed, *J. Phys. Chem. B* **2006**, *110*, 7238.
[43] M. Morita, T. Ohmi, E. Hasegawa, M. Kawakami, M. Ohwada, *J. Appl. Phys.* **1990**, *68*, 1272.
[44] P. R. Griffiths, J. A. d. Haseth, *Transform Infrared Spectrometry*, John Wiley & Sons, New Jersey **2007**.
[45] P. T. Boggs, J. E. Rogers, *Contemp. Math.* **1990**, *112*, 186.